BBA - Proteins and Proteomics 1867 (2019) 140254

Contents lists available at ScienceDirect

BBA - Proteins and Proteomics

journal homepage: www.elsevier.com/locate/bbapap

Exploring iron-binding to human frataxin and to selected Friedreich ataxia mutants by means of NMR and EPR spectroscopies

Massimo Bellanda[a,1], Lorenzo Maso[b,1], Davide Doni[b], Marco Bortolus[a], Edith De Rosa[a,b], Federica Lunardi[a], Arianna Alfonsi[a], Martín Ezequiel Noguera[c,d], Maria Georgina Herrera[c,d], Javier Santos[c,d], Donatella Carbonera[a,*], Paola Costantini[b,*]

[a] Department of Chemical Sciences, University of Padova, Via F. Marzolo 1, 35131 Padova, Italy
[b] Department of Biology, University of Padova, Viale G. Colombo 3, 35131 Padova, Italy
[c] Departamento de Fisiología y Biología Molecular y Celular, Facultad de Ciencia Exactas y Naturales, Universidad de Buenos Aires, Instituto de Biociencias, Biotecnología y Biomedicina (iB3), Intendente Güiraldes 2160 - Ciudad Universitaria, 1428EGA C.A.B.A., Argentina
[d] Intituto de Química y Fisicoquímica Biológicas, Dr. Alejandro Paladini, Universidad de Buenos Aires, CONICET, Junín 956, 1113AAD C.A.B.A., Argentina

ARTICLE INFO

Keywords:
Friedreich ataxia
Frataxin
Iron
FeS clusters assembly

ABSTRACT

The neurodegenerative disease Friedreich ataxia results from a deficiency of frataxin, a mitochondrial protein. Most patients have a GAA expansion in the first intron of both alleles of frataxin gene, whereas a minority of them are heterozygous for the expansion and contain a mutation in the other allele. Frataxin has been claimed to participate in iron homeostasis and biosynthesis of FeS clusters, however its role in both pathways is not unequivocally defined. In this work we combined different advanced spectroscopic analyses to explore the iron-binding properties of human frataxin, as isolated and at the FeS clusters assembly machinery. For the first time we used EPR spectroscopy to address this key issue providing clear evidence of the formation of a complex with a low symmetry coordination of the metal ion. By 2D NMR, we confirmed that iron can be bound in both oxidation states, a controversial issue, and, in addition, we were able to point out a transient interaction of frataxin with a N-terminal 6his-tagged variant of ISCU, the scaffold protein of the FeS clusters assembly machinery. To obtain insights on structure/function relationships relevant to understand the disease molecular mechanism(s), we extended our studies to four clinical frataxin mutants. All variants showed a moderate to strong impairment in their ability to activate the FeS cluster assembly machinery *in vitro*, while keeping the same iron-binding features of the wild type protein. This supports the multifunctional nature of frataxin and the complex biochemical consequences of its mutations.

1. Introduction

Frataxin (FXN) is a small highly conserved protein, found in both prokaryotic and eukaryotic organisms [1,2], that was originally identified based on its link to Friedreich ataxia (FRDA; OMIM 229300), a neurodegenerative disease caused by an abnormal expansion of a GAA repeat in the first intron of the *FXN* gene, leading to a severe deficiency of the protein [3,4]. FRDA is the most common inherited form of ataxia, clinically characterized by a progressive limb and gait ataxia, diabetes mellitus and hypertrophic cardiomyopathy, which is the main cause of death [5]. Although the majority of FRDA patients (*i.e.* > 95%) are homozygous for the GAA expansion, a small but significant proportion of them (*i.e.* around 4%) are compound heterozygous for the expansion on one *FXN* allele and for a mutation on the other, including nonsense, missense, insertion and deletions [6,7]. To date, out of the 40 reported pathogenic variants of FXN, at least 20 different point mutations have been described, and it is worth noting that all clinically important mutations described in heterozygous FRDA patients affect highly conserved residues [6]. These patients present either the classical FRDA phenotype or an atypical, less severe clinical picture [6,8]. Contrary to the homozygous GAA expansion, which reduces FXN levels, these missense mutations are expected to directly affect the activity and/or structural properties of the expressed protein, as suggested by *in vitro* studies using recombinant mutant proteins [9,10]. There are currently no options to prevent or specifically treat this disease, and life expectancy of patients is reduced to ~ 40–50 years. In fact, although

* Corresponding authors.
E-mail addresses: donatella.carbonera@unipd.it (D. Carbonera), paola.costantini@unipd.it (P. Costantini).
[1] These authors contributed equally to this work.

https://doi.org/10.1016/j.bbapap.2019.07.007
Received 12 March 2019; Received in revised form 12 July 2019; Accepted 18 July 2019
Available online 22 July 2019

FRDA has been unequivocally associated to FXN depletion, a clear cause-effect relationship is still elusive: the precise physiological function of the protein has not been clarified, as well as its specific contribution to the pathology onset and progression of both classical and atypical FRDA. Several potential roles have been proposed for FXN (reviewed in [11,12]), essentially based on the structural/functional features of the protein. Genetic and biochemical studies carried out on several orthologues support a role of FXN as a multifunction protein involved in different (and likely related) aspects of intracellular iron metabolism, ranging from biogenesis of heme [13] and FeS clusters [14], to iron binding/storage [15] and iron chaperon activity [16]. All these possible functions of FXN are in agreement with the cardinal downstream biochemical features of FRDA cells, *i.e.* an impaired mitochondrial respiration, likely due to the decrease of the FeS clusters working as electrons shuttles through the respiratory chain, associated to iron overload and increased sensitivity to oxidative stress [17–19]. Some of these defects are probably secondary consequences of FeS clusters assembly defects, and a large body of data supports the idea that the complex phenotypes associated with FXN deficiency in humans as well as in other eukaryotes reflects, at least in part, an impaired capability to assemble these key cofactors (as reviewed in [20]). In fact, FXN depletion is associated with multiple deficit of FeS proteins, especially mitochondrial aconitase and respiratory chain complexes [17] but also cytosolic enzymes [21]; this is usually accompanied by a general dysregulation of cellular iron homeostasis, leading to mitochondrial iron accumulation and cytosolic iron depletion [22,23]. It is thus generally accepted that FXN is a mitochondrial protein involved in iron metabolism, however whether and how it directly participates in this pathway remains unclear and controversial.

Human FXN is a nuclear-encoded protein, ubiquitously expressed at low levels, with the higher concentrations found in tissues strongly dependent on respiratory metabolism, such as heart, dorsal root ganglia sensory neurons and spinal cord [3]. It is an acidic iron-binding protein [1], synthesized in the cytosol as a precursor of 210 amino acids and then imported to the mitochondrion, where it undergoes to proteolytic maturation by a two-step process leading to an intermediate form of 19 kDa (residues 42–210) and finally to a mature form of 14 kDa (residues 81–210) [24–26], which is widely accepted to be the most abundant species both in normal individuals and in patients. Sequence alignment of frataxins from different organisms showed two distinct regions: i) a N-terminal block of 70–90 residues, completely absent in prokaryotes and poorly conserved also among eukaryotes, with features typical of intrinsically unfolded proteins, and ii) a C-terminus encompassing a block of about 100–200 amino acids that is highly conserved in most organisms. The sequence identity of this region is as high as 25%, and the similarity is 40 to 70%, indicating that this is likely the functional portion of the protein. The three-dimensional crystal structure of a recombinant human FXN has been solved [27,28] and indicates that the protein has indeed a N-terminal tail (residues 81–92) intrinsically unfolded and highly flexible, and a C-terminal domain folded in a mixed, compact αβ-sandwich, with two α-helixes packing against an antiparallel β-sheet. Several highly conserved residues are buried in the protein core, consistent with a requirement for maintenance of a compact structure, whereas other are located either in a N-terminal anionic patch or within the flat, conserved external surface of the β-sheet, strongly supporting the hypothesis that these surfaces are critical for FXN function. The highly acidic N-terminal domain, corresponding to the first α-helix together with the first β-strand, has been suggested to confer to FXN the capability to bind iron, and indeed independent NMR studies on human, yeast and bacterial frataxin homologues indicated iron addition effects at or near the negatively charged residues (aspartate and glutamate) clustered on this surface acidic ridge [27,29–32]. On the other hand, there is still uncertainty with respect to the iron-stoichiometry and affinities as well as type of coordination: different constructs of human FXN were reported to bind different Fe^{2+}/Fe^{3+} equivalents per monomer, with largely discrepant dissociation constants [13,16,33], and it has been recently proposed that this protein is not able to bind ferric iron [34], making even more controversial its involvement in iron metabolism and homeostasis. Moreover, how the capability of human FXN to bind iron is related to its potential role in the FeS clusters assembly process is not completely clarified and unequivocally defined.

Based on these premises, in this work we combined different spectroscopic analyses to further characterize the iron-binding properties of human FXN, both as isolated and at the FeS clusters assembly machinery. Moreover, we extended our study to four variants found in FRDA heterozygous patients carrying clinically relevant missense mutations in highly conserved FXN residues.

2. Materials and methods

All chemicals were of the highest purity commercially available.

2.1. Heterologous expression and purification of human FXN, ISCU and NSF1/ISD11 proteins

A plasmid containing human wild type mature FXN, *i.e.* pET-9b/FXN(90–210), was previously obtained in our laboratory as described in [35]. FXN mutants were obtained through site-directed mutagenesis with the QuickChange® II Site-Directed Mutagenesis Kit (from Agilent Technologies), using as template the pET-9b/FXN(90–210) plasmid and the couples of primers listed in Table 1 (Supplementary material). The sequence of each mutant FXN gene was confirmed by DNA sequencing (at GATC Biotech, Germany). Human ISCU2 cDNA cloned into a pENTR223.1 vector was purchased from MyBioSource, Inc. (San Diego, CA, USA) and used as template to amplify the sequence corresponding to the mature ISCU2 variant, *i.e.* without mitochondrial targeting sequence, by using the couple of primers Fw_{ISCU} (5′-gaattcttatcaacaagaaggttgttgat-3′) and Rev_{ISCU} (5′-aagctttcatttcttctctgxctctcc-3′). The fragment of interest was then directionally sub-cloned into a pETDuet-1 expression vector in frame with a sequence coding for a 6his-tag at the 5′ terminus. The identity of the insert was confirmed by DNA sequencing (at GATC Biotech, Germany). The sequence coding for the mature ISCU2 protein was also sub-cloned in frame with the 6his-tag sequence at the 3′ terminus into a pET-22b(+) expression vector, also carrying the TEV protease cleavage site sequence to remove the 6his-tag from the C-terminus of the purified protein, as described in more detail in Supplementary material. Sequences coding for mature mouse NFS1 and ISD11 proteins were cloned into the two multi-cloning sites (*NFS1* in MCS1, in frame with a N-terminus 6his-tag, and *ISD11* in MCS2) of a pETDuet-1 vector. *Escherichia coli* BL21 (DE3) cells were transformed with the plasmids of interest, positive clones selected by antibiotic resistance, and recombinant proteins expressed and purified as described in more detail in Supplementary material: briefly, 6his-ISCU2 by combining affinity Ni-NTA and size exclusion chromatographies, wild type and mutant FXN proteins by combining anion exchange and size exclusion chromatographies, and the NFS1/ISD11 complex by a single step of Ni-NTA affinity chromatography, exploiting the NFS1 N-terminus 6his-tag.

2.2. Cysteine desulfurase activity measurements

The enzymatic catalysis of cysteine to alanine by NFS1/ISD11 (SD) complex was measured by the production of sulfide, using slight modifications of the assay described by Leimkühler and co-workers [36]. Briefly, sulfide quantification was performed by a colorimetric reaction in which the latter is used to generate methylene blue. For the assay, a total volume of 0.4 mL was employed, containing 1 μM NFS1/ISD11, 3 μM FXN and 3 μM ISCU. The samples were also supplemented with 10 μM PLP, 2 mM DTT and 10 μM Fe^{2+} at final concentrations. Argon-purged 50 mM Tris-HCl, 200 mM NaCl, pH 8.0 was used as the reaction buffer. To initiate the reaction, 1 mM cysteine was added and

the sample was incubated at room temperature. As sulfide production is linear during the first 40 min (data not shown), 30 min were employed to generate sufficient product for the detection. The assays were stopped by the addition of 50 μL of 20 mM *N*,*N*-dimethyl *p*-phenylenediamine in 7.2 M HCl and 50 μL of 30 mM $FeCl_3$ in 1.2 M HCl. After letting the reaction proceed for 20 min, the samples were centrifuged for 5 min at 12000 x*g*. Then, the absorbance at 670 nm was measured. The same assay was performed for each frataxin variant, in the same concentration as the wild type. In this case, the desulfurase activity was normalized to the activity of the wild type protein.

2.3. Circular dichroism (CD)

CD measurements were performed with a Jasco J-810 spectropolarimeter. Far-UV CD spectra were collected using cells of 0.1 cm path-length. Data were acquired at a scan speed of 20 nm/min and at least three scans were averaged. Proteins were used at a concentration of 0.2 mg/mL, in a 2.5 mM Tris-HCl pH 7.0, 5 mM KCl buffer. Experiments were performed at 25 °C using a thermostated Jasco PTC-423 peltier cell holder connected to a Jasco PTC-423S peltier controller. The secondary structure content of all analyzed proteins was calculated using the CD spectrum deconvolution software CDNN (a software that calculates the secondary structure by comparison with a CD database of known protein structures) [37], and then compared with the one present in literature to confirm their correct folding state.

2.4. UV–Vis absorption and fluorescence spectroscopy

UV–Vis absorption were performed using a Cary 100 UV–Vis Spectrometer from Varian. Fluorescence spectra were detected with a FluoroMax-P Fluorimeter from Horiba Scientific, using 280 nm excitation wavelength which allows to excite tryptophan residues. Quartz cells of 1 cm path-length were used. Proteins were used at a concentration of 0.05 mg/mL (10 μM), in a 100 mM HEPES pH 7.5, 50 mM KCl buffer. Experiments were performed at 25 °C using a thermostated cell. Fe^{3+} equivalents were added step by step starting from a concentrated stock solution of $FeCl_3$ in diluted HCl (pH ~ 2) by addition of few microliters each time, under constant stirring. Correction of the fluorescence spectra for the filter effect and for dilution resulted to be negligible.

2.5. Electron paramagnetic resonance (EPR) spectroscopy

EPR spectra were recorded on an ELEXSYS E580 spectrometer equipped with a rectangular cavity, ER4102ST, both from Bruker, Germany, and fitted with a cryostat (ESR900) and a variable-temperature controller (ITC503S), both from Oxford Instruments, UK. The experiments were performed using the following parameters: microwave frequency 9.38 GHz, microwave power 6.4 mW (attenuation 15 dB), sweep width 170 mT, center field 150 mT, conversion time 82 ms, time constant 41 ms, modulation amplitude 0.95 mT, 1024 points, 50 averages, temperature 10 K. Samples were prepared incubating the proteins and 2 μL of Fe^{3+} in a FXN:Fe^{3+} 1:4 molar ratio and a final protein concentration 50 μM, in a 25 mM HEPES pH 7.0, 5 mM KCl buffer, sample volume 100 μL. Fe^{3+} was added from a concentrated solution stock solution of $FeCl_3$ in diluted HCl (pH ~ 2), [Fe^{3+}] = 10 mM. Samples were frozen in dry ice in quartz tubes (i.d. 3 mm, o.d. 4 mm). Quantitative measurements were performed for all samples using identical instrumental conditions, volume and position of the sample tube. The spectra were corrected by subtracting the baseline obtained from the spectrum of a solution of 200 μM Fe^{3+} in buffer.

2.6. Nuclear magnetic resonance (NMR) spectroscopy

Wild type and mutant FXN ^{15}N-labeled and $^{15}N/^{13}C$-double labeled proteins were isolated from *E. coli* cultures expressing the protein of interest, grown in M9 minimal media supplemented with ^{15}N $NH_4Cl/^{13}C$ D-Glucose, in the same conditions described above. When Fe^{2+} was used, all samples were prepared with N_2 purged buffer (25 mM Tris-HCl pH 7.0, 50 mM KCl, and 1 mM DTT) under an anaerobic glove box (MBRAUN MB-200B) saturated with N_2. ^{15}N labeled wild type and mutant FXN proteins had a final concentration of 45 μM; unlabeled ISCU, when present, was at 80 μM, taking into account that in all ISCU sample preparations a complex SEC profile was observed, indicative of the co-existence of monomeric and dimeric proteins, or of species with different degree of folding. Fe^{2+} stock solution was freshly prepared before each experiment, dissolving $(NH_4)_2Fe(SO_4)_2{\cdot}6H_2O$ in the buffer described above, into the anaerobic glove box. Fe^{3+} solution was prepared dissolving $FeCl_3$ in the same buffer. Both iron stock solutions had a concentration of 14 mM. Samples "FXN wild type/mutant + Fe" (1:4 FXN:Fe ratio) and "FXN wild type/mutant + Fe + ISCU" (1:4:2 FXN:Fe:ISCU ratio) were prepared starting from a common stock of FXN wild type/mutant + Fe, and then diluted to the right final concentration either with buffer alone or with buffer + ISCU, in order to obtain the same FXN/Fe ratio in all experiments. 10% D_2O was added to all samples, which were then transferred in anaerobic conditions in Shigemi NMR tubes, without the insert, and sealed with appropriate rubber septa that secured air-tightness throughout the duration of the experiments. Before and after NMR experiments, pH of all samples was strictly controlled, and, in particular after addition of Fe^{3+}, it was necessary to adjust it with 1 M NaOH. All NMR experiments were acquired at 298 K on a Bruker DMX 600 MHz spectrometer with room temperature probes. SOFAST HMQC (band-Selective Optimized Flip-Angle Short-Transient Heteronuclear Multiple Quantum Coherence) [38] was used to monitor the effect of iron and ISCU on ^{15}N labeled FXN wild type/mutants. Resonance assignment for the amides groups of FXN was achieved by comparison with data available for human FXN in the BMRB database (http://www.bmrb.wisc.edu; accession code: 4342) and confirmed by HNCA, HN(CO)CA, HNCO, HN(CA)CO, HNCACB and HN(CO)CACB 3D heteronuclear experiments, using a sample of 1 mM doubly-labeled protein in the same buffer described above. Spectra were analyzed with NMRFAM-Sparky 1.4 [39] and CARA [40]. Normalized chemical shifts were calculated using the following the equation:

$$\Delta\delta = ((\delta_{HN})^2 + (\delta_N/5)^2)^{0.5}$$

Residues that underwent significant chemical shift perturbations were mapped on the human FXN crystal structure (PDBID: 1EKG) using the program PyMOL [41].

3. Results and discussion

Despite the wide consensus that frataxins are iron-binding proteins involved in the mitochondrial FeS clusters assembly process, there is not a general agreement on iron stoichiometries and dissociation rates, nor on the specific role of frataxin either in the FeS clusters biogenesis or in iron homeostasis. This issue is even more complex for human FXN, for which different recombinant constructs have been shown to bind 6 to 7 iron ions per monomer, irrespective of whether they were Fe^{2+} or Fe^{3+} [16,33,42], with largely incongruous dissociation constants. It is worth noting that in many respects frataxins are quite atypical iron-binding proteins, since they are thought to achieve iron coordination solely through aspartate and glutamate residues exposed on the protein surface instead of cysteines as most of the other iron-binding proteins. An additional unusual property, which may contribute to the experimental discrepancies, is related to the apparent lack of selectivity of frataxin, which is able to coordinate most divalent cations using the same surface acidic residues used for iron [43], so that different experimental conditions could in principle affect both stoichiometries and measured dissociation constants. Moreover, although eukaryotic $FXN_{81–210}$ is widely accepted as the mitochondrial mature form and several experimental data refer to this protein, pivotal structural studies

have been performed with a shorter construct (*i.e.* $FXN_{90–210}$), which comprises only the C-terminal evolutionary conserved domain and lacks the extra stretch of residues besides the mitochondrial import sequence at the N-terminus, that is likely unfolded [16,27,29,44]. In the first part of this work, we readdressed the iron-binding properties of a recombinant human $FXN_{90–210}$ protein by means of a multidisciplinary approach in which different spectroscopic analyses have been combined to obtain new independent structural data on the controversial role of iron in frataxin function(s). Moreover, to gain new clues on potential structure-function relationships, we extended our studies to a panel of selected FXN clinical variants carrying a point mutation either in the iron-binding region itself (*i.e.* D122Y) or in the conserved external surface likely involved in the interaction with the FeS clusters assembly machinery (*i.e.* G130V, N146K and W155R). In the second part of the work, we focused on the iron effect in relation to the structural and functional interactions of these FXN constructs with the FeS clusters assembly machinery, in order to obtain additional molecular details on the involvement of FXN in this biosynthetic pathway.

3.1. Testing iron-binding to human FXN and to selected clinical variants found in FRDA patients

3.1.1. Heterologous expression and purification of different variants of human $FXN_{90–210}$

We overexpressed in *E. coli* and purified by combining an anionic exchange and a size exclusion chromatography, as described in detail in the section Materials and methods, both the wild type $FXN_{90–210}$ protein (supplementary Fig. S1) and the four clinical variants (not shown), obtained by inserting the selected point mutation into the wild type $FXN_{90–210}$ coding sequence by site-specific mutagenesis. All $FXN_{90–210}$ variants were expressed at the same extent as the wild type protein and were almost completely found in the soluble fraction after cell lysis, except for G130V mutant, which showed a higher tendency towards aggregation (supplementary Fig. S2), as previously reported by Correia and coworkers [9]. This could be explained by the position of residue G130, which is in the tight turn formed by G128, S129 and G130 itself, between strands β1 and β2; thus, its mutation into a valine may disturb the turn conformation, resulting in a severe local strain.

3.1.2. UV–visible and fluorescence spectroscopy

The oxidation of Fe^{2+} in the presence of FXN was estimated by following the absorbance change at a wavelength of about 296 nm, which is diagnostic of formation of oxo/hydroxo Fe^{3+} species [45], after adding Fe^{2+} to the protein in aerobic buffer, without stirring. The oxidation rate, in these conditions, depends on the Fe^{2+}/protein ratio. While at low iron concentration the oxidation rate is lower than that of the auto-oxidation in buffer, at higher equivalents the oxidation occurs at rates faster. In fact, after adding 3 equivalents, corresponding to 30 μM of Fe(II), the oxidation rate is already much faster compared to auto-oxidation of Fe^{2+} in buffer at the same iron concentration (Fig. 1). Moreover, there is a fast (within the 10–20 s) initial oxidation phase clearly observable by adding 3 or more iron equivalents, followed by a slower oxidation process. The fast oxidation is saturating already at about 3–4 Fe^{2+} equivalents, showing the same optical density change by addition of 10 equivalents. The second phase is dependent on the Fe^{2+} concentration as expected for an enzymatic reaction following the Michaelis-Menten relationship. Clearly, as the titration progresses, iron-binding sites with different reaction properties are filled. A similar behavior was reported before for CyaY from *E. coli* [45] and was ascribed to the presence of different iron-binding sites.

An indirect evidence for the iron-FXN complex formation was then provided by fluorescence quenching of the tryptophan residues emission, induced by Fe^{3+} addition to a protein solution. The effect on the fluorescence may mainly be ascribed to the energy transfer of the excitation that occurs between tryptophan residues and the oxo-complexes formed by Fe^{3+} ions with the protein upon binding, as suggested

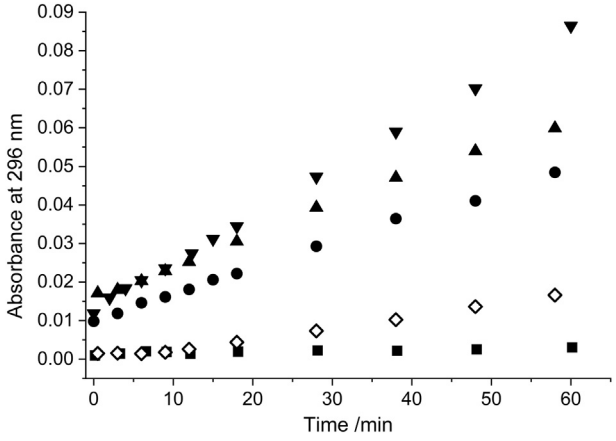

Fig. 1. Kinetics of Fe^{2+} oxidation. The oxidation of Fe^{2+} to Fe^{3+} was detected by absorbance change at 296 nm, at different FXN: Fe^{2+} molar ratios: squares, 1:0.5; circles, 1:3; up triangles, 1:4; down triangles, 1:10. In empty diamonds, the oxidation in buffer alone of Fe^{2+} 30 μM. Protein concentration: 10 μM. $T = 298$ K.

before for ferritin fluorescence quenching observed when Fe^{3+} was loaded [46]. Human FXN contains three tryptophan residues, and it is worth noting that one of them is missing in one of the four variants analyzed in this work (*i.e.* the W155R FXN). It can be seen that the fluorescence quenching due to the increasing amount of ferric ions is similar among the samples (wild type and mutants), with a more pronounced deviation for the D122Y mutant, which shows a reduced quenching (about −20%) (Fig. 2). The quenching of fluorescence produced by Fe^{2+} was almost absent (data not shown). In the case of Fe^{2+} the quenching, strongly reduced compared to that induced by Fe^{3+} addition, is expected to be due only to a paramagnetic effect rather than to energy transfer as for Fe^{3+}. However, since strictly anaerobic conditions were not guaranteed, it is possible that the observed quenching derives from the trace amounts of Fe^{3+} produced by oxidation due to the residual oxygen. Our experimental data on Fe^{2+} are in disagreement with those reported by Yoon and co-workers, who observed a large fluorescence quenching following Fe^{2+} addition, similar to that observed with Fe^{3+} [13].

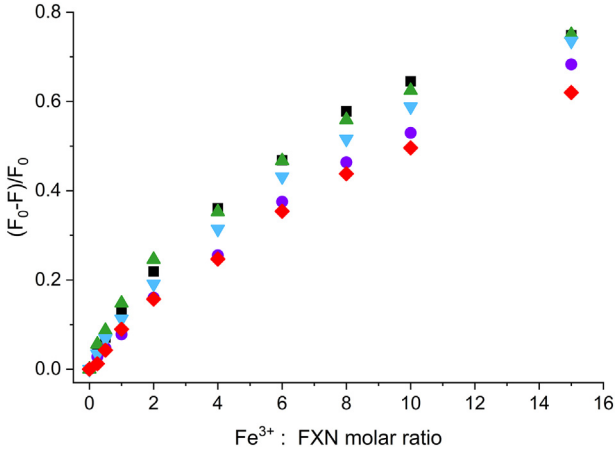

Fig. 2. Quenching of tryptophan fluorescence intensity in wild type and mutant FXN proteins after addition of increasing Fe^{3+} equivalents. The quenching was followed on the maximum of fluorescence emission at different FXN:Fe^{3+} molar ratios. Black squares, wild type FXN; red diamonds, D122Y mutant; purple circles, G130V mutant; azure down triangles, N146K mutant; green up triangles W155R mutant. F = fluorescence intensity at the actual concentration of Fe^{3+}, F_0 = fluorescence intensity in the absence of Fe^{3+}. Protein concentration: 10 μM. T = 298 K.

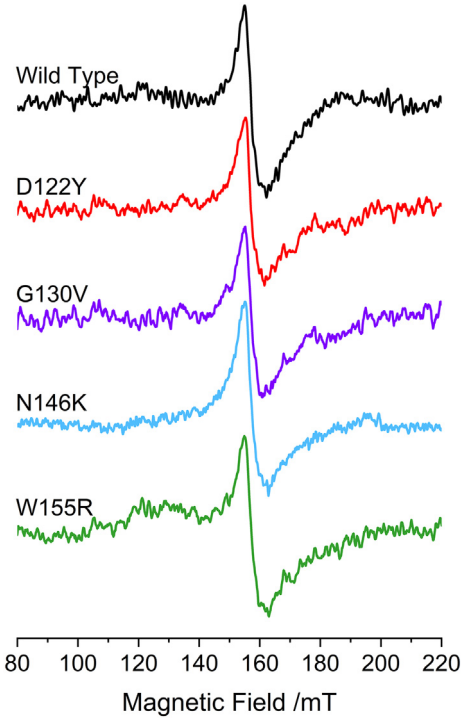

Fig. 3. EPR spectra of Fe^{3+} bound to wild type and mutant FXN proteins. The spectra show the g = 4.3 spectral region. Top to bottom: black, wild type FXN; red, D122Y mutant; purple, G130V mutant; azure, N146K mutant; green, W155R mutant. The samples have a 4:1 Fe^{3+}:FXN ratio. Protein concentration: 50 μM. T = 10 K.

The iron-binding to FXN was further addressed, for the first time, by EPR spectroscopy of wild type and mutant frataxins, as described in the following.

3.1.3. EPR spectroscopy

EPR measurements were performed at 10 K to get a direct evidence, instead of an indirect effect as probed by fluorescence spectroscopy, of the iron-binding to FXN, since EPR is able to detect bound Fe^{3+} ions and gives information on the coordination to the protein residues. A protein sample in the absence of iron does not show an EPR signal, and the signal of Fe^{3+} in HEPES buffer solution at pH 7.0 is negligible in the low-field g = 4.3 region and absent at higher field values (data not shown). This was expected, since i) HEPES does not coordinate iron and ii) under these experimental conditions, in terms of pH and concentration, iron precipitates as hydroxide. On the other hand, when Fe^{3+} was added to FXN, a signal centered at g = 4.3, ascribed to a high-spin mononuclear Fe^{3+} species in an environment of low symmetry, has been observed for all the samples, compatible with an aspartate/glutamate coordination [47], with no further signals present in other spectral regions. In Fig. 3, the EPR signals detected after addition of 4 equivalents of Fe^{3+} to 50 μM protein solutions are shown. The spectra have been normalized to unit intensity to compare their shape: no significant differences among the samples have been detected when comparing wild type and mutant frataxins. The intensity of the signal of D122Y variant was reduced with respect to that of the wild type, in agreement with the fluorescence experiments reported above. Instead, the other variants showed only slightly different signal intensities.

The EPR experiments unequivocally show that i) FXN is able to bind Fe^{3+} ions and ii) the mutations in the FXN clinical variants examined in our study do not impair the protein ability to bind iron ions. The D122Y mutant seems to be affected in this respect, but the capability of binding iron is not fully compromised. Due to the broadness of the spectral shape, it was not possible to characterize the different iron-binding sites suggested by the absorption spectra.

We next investigated the iron-binding properties of wild type and mutant frataxins by NMR, either as isolated and in the presence of ISCU, the key scaffold protein of the FeS clusters assembly machinery.

3.1.4. 2D NMR analysis

Both the NMR spectral assignment and the structure of human $FXN_{90–210}$ have been previously achieved by Musco and coworkers [27,44], and the Fe^{2+}-binding sites were mapped onto the protein by chemical shift perturbation analysis [29]. We first confirmed these data by titrating with Fe^{2+} a ^{15}N-labeled $FXN_{90–210}$ protein and using SO-FAST-HMQC NMR spectra to monitor perturbations, as described in detail in Material and methods, and we performed the same analyses with Fe^{3+}. Supplementary Fig. S3 shows the NMR spectrum of FXN with the peak assignments, whereas supplementary Fig. S4 reports the superimposition of the spectra in the absence and in the presence of Fe^{2+} (panel A) or Fe^{3+} (panel B). In these experiments we used a protein:iron ratio of 1:4 and at the relatively low FXN concentration used in our experiments we did not observe any evident precipitation upon addition of Fe^{3+}. Fig. 4, panels A and B, shows the normalized chemical shift changes, calculated as described in Materials and methods. Upon the addition of Fe^{2+} in anaerobic conditions (panel A), as previously shown [29], or of Fe^{3+} (panel B), positions and/or intensities of several peaks in NMR spectra of FXN resulted to be perturbed. As expected, the perturbed peaks mostly correspond to residues belonging to the N-terminal α1/β1 acidic iron-binding region of FXN. Titration of FXN with Fe^{3+} showed effects qualitatively similar to those caused by Fe^{2+}, indicating that the protein binds iron ions by using essentially the same area, as previously reported for the frataxin bacterial homologue CyaY [29]. Interestingly, Fe^{2+} generally induces larger perturbations (larger shifts or higher intensity decrease of the peaks), except for residues 119 and 120, that appear more shifted upon addition of Fe^{3+} (Fig. 4, panels A and B). This is in agreement with the EPR data reported above, showing that Fe^{3+} is able to bind to FXN, and further suggests a slightly different binding mode for iron in the two oxidation states.

We next analyzed, in the same experimental conditions, the 2D NMR spectra of the four clinical FXN variants described above, either in the absence or in the presence of Fe^{2+}. The same experiment using Fe^{3+} was not performed because of the very similar effects observed on wild type FXN upon addition of iron in the two different oxidation states. In the absence of iron, the spectra of all mutants showed a good signal dispersion, compatible with folded species (supplementary Fig. S5). This was already reported for D122Y, G130V and W155R [9] but not for N146K, whose $^{1}H–^{15}N$ correlation spectrum is shown here for the first time. All the spectra of the mutants were partially superimposable to that of the wild type protein and, accordingly, it was possible to assign most of the resonances and to identify the regions most perturbed by the mutations (supplementary Fig. S6). When compared to the wild type protein, the NMR spectra of the four clinical FXN variants reflected local rearrangements, mostly surrounding the mutation. In all cases some peaks of residues adjacent to the mutation could not be assigned because of very large shifts when compared to the wild type protein. For mutant D122Y, the substitution induced strong perturbations in several residues facing it. Perturbed regions include residues of the terminal part of α1 and the beginning of β1 together with the loop connecting them, the loop between β1 and β2 and the beginning of α2. The most significant perturbations were observed for the G130V and W155R variants, in a relatively wide region extending from the mutation that includes not only residues from the whole β-sheet but also from the N-terminal part of α1, as shown in supplementary Fig. S6. These results are compatible with the W155R crystal structure, in which a significant side-chain reorganization surrounding the mutation is evident when compared to the native FXN [48]. Instead, mutation N146K perturbed only few adjacent residues, mostly belonging to β3 (where mutation is located) and β4 strands (supplementary Fig. S6).

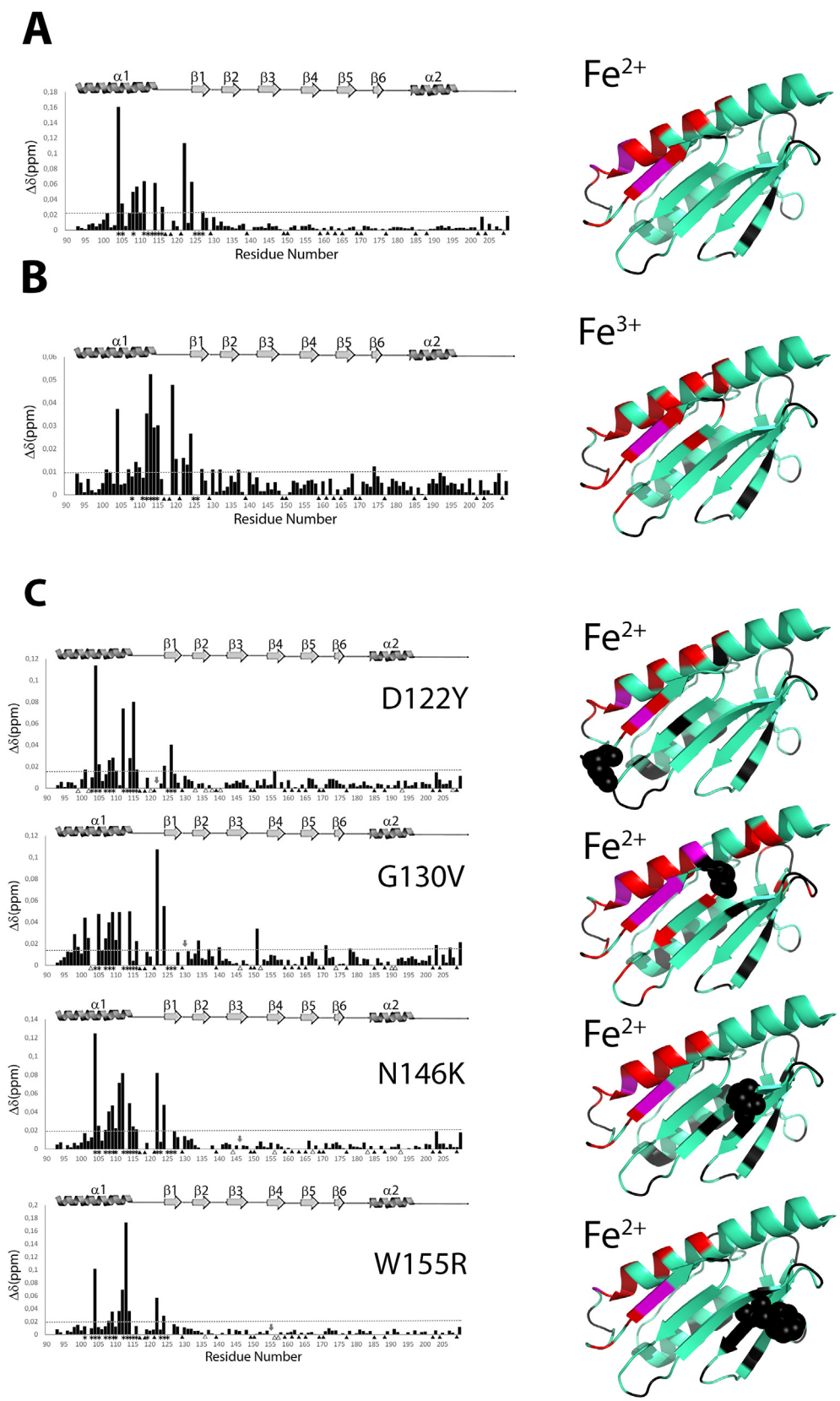

Fig. 4. Mapping the iron-binding sites of FXN by NMR chemical shift perturbation. Normalized chemical shift changes for wild type FXN with and without 4 equivalents of Fe^{2+} (A) or Fe^{3+} (B) and for the four FXN mutants with and without 4 equivalents of Fe^{2+} (C). The dotted line represents the threshold calculated as one standard deviation of the shifts. The asterisks indicate residues whose peaks disappeared or presented significantly reduced intensity in presence of iron. Prolines or residues corresponding to severe overlapped or unassigned peaks in wild type FXN are indicated with black triangles while residues which cannot be traced in the mutants are shown with empty triangles. A schematic representation of FXN secondary structure is inserted in frame with residues sequence number to facilitate the interpretation of the figure. On the right column, protein regions perturbed upon iron addition are mapped with colours on the apo-FXN structure (PDBID: 1EKG). The residues presenting, upon addition of iron, normalized chemical shift changes larger than a one standard deviation of all the shifts are coloured in red. Residues whose signal disappear upon addition of iron are coloured in magenta. The mutated residues are represented in spheres. In black are coloured prolines, residues corresponding to severe overlapped or unassigned peaks in wild type FXN and residues whose assignment could not be traced in the mutants.

This is in agreement with the crystal structure of the variant N146K (construct $FXN_{90–210}$), that shows backbone and side chain conformations similar to those of native FXN [9]. Additionally, we analyzed the temperature-induced unfolding profiles of all FXN variants (as assessed by using Sypro-orange dye that binds to the unfolded state) and found T_m values compatible with stable tertiary structure and resistance to the temperature unfolding, *i.e.* 50.3 ± 0.3, 57.1 ± 0.3, 54.8 ± 0.1, 69.4 ± 0.1, 64.9 ± 0.2 °C for G130V, D122Y, W155R, N146K and wild type FXN, respectively (Fig. 5). Interestingly, mutation N146K may be stabilizing. On the other hand, since a difference in T_m does not

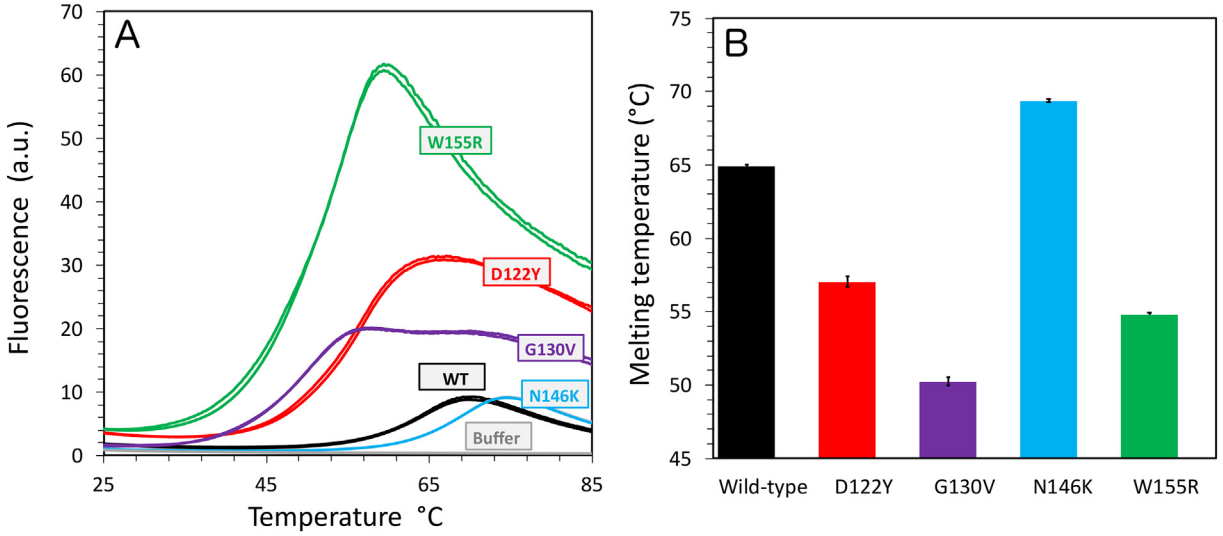

Fig. 5. Temperature-induced unfolding of FXN mutants. Unfolding of FXN mutants was followed by the change in sypro-orange dye fluorescence. (A) Unfolding profiles. (B) Melting temperatures. Data represent the mean of four replicates ± S.D. for each variant.

necessarily imply a difference in free energy more experiments will be carried out in order to confirm these data.

We then explored by the same NMR analysis the N-terminal acidic region of these four clinical variants after addition of Fe^{2+} at a 1:4 protein:iron ratio. Notably, in these conditions, for the W155R mutant we did not observe any significant protein precipitation as was previously reported [9], most likely due to the lower protein concentrations used in our experiments. The results are shown in Fig. 4, panel C, which reports the normalized chemical shift and intensity changes (NMR spectra are in supplementary Fig. S7). When compared to the wild type protein, FXN variants showed similar behaviors in the presence of four equivalents of Fe^{2+}. The iron-binding region of mutants N146K and W155R resulted to be almost identical to that of the wild type protein, suggesting that these two mutations do not significantly impact on the iron-binding capability of FXN. Instead, the effect of Fe^{2+} on the NMR spectrum of mutant G130V involves a larger number of peaks which become very broad or shift, with additional perturbed residues surrounding the α1/β1 acidic region. This increased perturbation in the NMR spectrum of G130V FXN variant upon addition of Fe^{2+} could reflect the lower conformational stability previously observed by Correia and coworkers [9], as discussed above, and it is in agreement with a decrease in T_m value compared to the wild type FXN (ΔT_m = 14.6 °C). Surprisingly, with four Fe^{2+} equivalents, mutant D122Y does not show striking differences in the iron-binding region, where the mutation is located, when compared to the wild type protein. On the other hand, it must be underlined that residues 120 and 121 (and 122 itself) were not assigned in this mutant because of their large resonance shift; thus, possible differences in this region potentially affecting the capability of D122Y FXN variant to bind iron could not be tracked. As the EPR and fluorescence experiments reported above suggest, at least for Fe^{3+} binding, D122Y FXN shows a reduced capability to bind iron with respect to all the mutants addressed in this work. This is in agreement with the previous observation that iron-binding is only partially impaired in this mutant, which maintains the ability to bind four irons per protein.

An additional key open issue is the way by which FXN is involved in the FeS clusters assembly process; several functions have been hypothesized for FXN in this pathway, ranging from iron delivery [16,49,50] to allosteric activation of the assembly machinery [51–53]. However, a converging consensus on its specific role is still missing. We thus further investigated this issue, focusing on the structural and functional interactions of FXN with ISCU, the scaffold protein upon which the FeS clusters are assembled prior to the transfer to the target apoproteins, as reported in the next paragraph. Although we used the mitochondrial isoform ISCU2, this protein will be simply referred as ISCU in the following.

3.2. Exploring human iron-bound FXN at the FeS cluster assembly machinery

According to an involvement in the FeS clusters biogenesis, human FXN was shown to interact with multiple core components of the assembly machinery. In eukaryotes, FeS proteins are distributed in almost every cellular compartment, especially in mitochondria, cytosol and nucleus [54]; the assembly of the FeS clusters is mainly performed by the mitochondrial ISC multiprotein machinery, which is composed of the cysteine desulfurase NFS1, the accessory proteins ISD11 and ACP (Acyl Carrier Protein), and the ISCU scaffold [55–60]. It is worth noting that although eukaryotes possess an additional cytosolic assembly system (*i.e.* CIA, Cytosolic Iron-sulfur cluster Assembly) [54], the ISC complex is also essential to all extra-mitochondrial FeS proteins [54,55], putting this machinery more in general at the core of the metabolic pathways involving FeS proteins, both in healthy cells and in human diseases caused by FeS clusters deficiencies, including Friedreich ataxia. Although evidence of an interaction between FXN and the NFS1-ISD11-ACP-ISCU complex has received many independent confirmations [34,49,53,61–64], several questions are unanswered, particularly as far as concerns its direct partner, which remains controversial as different one-to-one interactions with each component were reported [16,49,61,63,64]. It is worth noting that many residues of the FXN whole β-sheet external surface are highly conserved and have been claimed to be critical for its specific interactions with other FeS cluster assembly proteins [28,62]. Several known missense point mutations associated with compound heterozygous FRDA patients map indeed to these residues, including the four selected for our study, that belong either to the N-terminal anionic patch or to the flat, conserved external surface of the β-sheet, which is likely fundamental for the docking of protein partner(s) on FXN.

Whatever is the specific role of FXN, the general consensus is that it is iron-dependent [16,34,49], and that it relies on transient interactions with the biosynthetic core complex. Thus, by means of the same NMR analysis described above, we addressed the iron-binding to FXN in the presence of the scaffold ISCU, using either the wild type protein or the four selected pathological mutants. To this end, we heterologously expressed and purified a recombinant human mature (*i.e.* without the N-terminal mitochondrial targeting sequence) N-6his-tagged ISCU

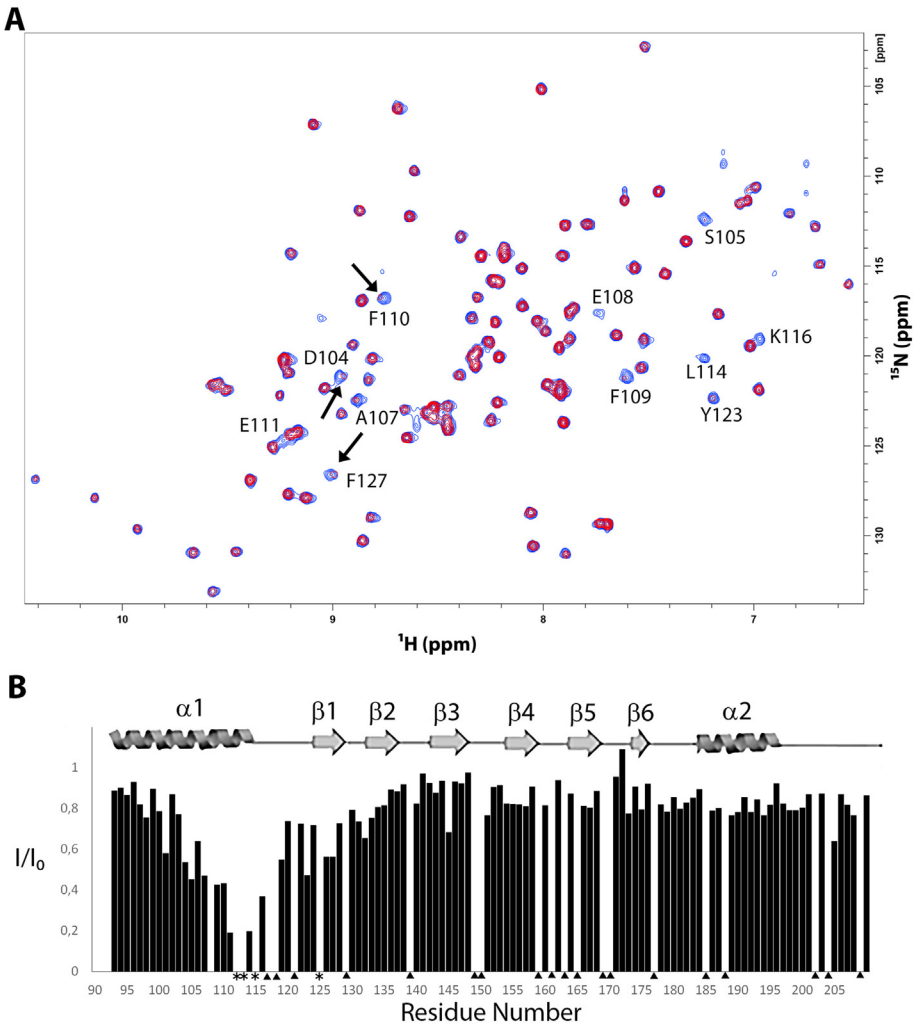

Fig. 6. Effect of N-6his-tagged ISCU on the NMR spectra of FXN in presence of four equivalents of Fe^{2+}. The superposition of the ^{1}H,^{15}N-SOFAST-HMQC spectra of FXN in absence (blue) and in presence (red) of ISCU are shown in panel A. The ratios of the peak intensities in the spectra without (I_0) and with (I) ISCU are represented as a function of the residue number in panel B. Residues corresponding to signals which disappeared in presence of ISCU and iron are indicated with asterisks. Prolines or residues corresponding to severe overlapped or unassigned peaks in wild type FXN are marked with black triangles. A schematic representation of FXN secondary structure is inserted in frame with residues sequence number to facilitate the interpretation of the figure. The black arrows indicate peaks that, besides being broadened, are also slightly shifted upon addition of ISCU.

protein, as described in detail in Materials and methods. The purified protein showed a secondary structure content compatible with a properly folded α/β species, as assessed by far-UV circular dichroism (supplementary Fig. S8 and Table 2 in Supplementary material). Addition of unlabeled ISCU to the ^{15}N-labeled FXN protein was then performed in the presence of Fe^{2+}, in anaerobic conditions, as described in detail in Material and methods, with a 1:4:2 FXN:Fe^{2+}:ISCU ratio. In order to facilitate the interaction with FXN, ISCU was added in excess taking into account that this protein is present in solution in monomeric and dimeric states, as pointed out above. The SOFAST HMQC NMR spectrum was finally acquired to map the residues potentially affected by the presence of ISCU. We found that addition of ISCU did not cause evident chemical shift perturbation on the NMR spectrum of the iron-bound frataxin (Fig. 6), which would have indicated the formation of a binary complex interaction of this protein with ISCU, at least in the absence of the other ISC complex functional partners. Interestingly, some cross-peaks corresponding to residues located in the α1/β1 acidic region already perturbed by iron-binding became significantly broader upon addition of N-6his-tagged ISCU. Furthermore, a close look to the NMR spectrum of the Fe^{2+}-bound FXN protein indicates that few residues present a small but significant shift in the proton dimension upon addition of ISCU (Fig. 6). In particular, the significant increase of line broadening for residues in the α1/β1 acidic region already perturbed by iron-binding could be due to an enhancement of paramagnetic relaxation caused by existence of transient, low population of the complex between the two proteins. Moreover, we added the N-6his tagged ISCU to ^{15}N-labeled frataxin in absence of iron and, as expected, in this case we did not observe any effect (supplementary Fig. S9), confirming that the further broadening is due to enhanced paramagnetic relaxation, which is very sensitive to protein-protein interaction. Although a strong interaction between the two proteins can be excluded, our data suggest that, even in the absence of the cysteine desulfurase complex, ISCU could interact directly with the α1/β1 acidic region or that a transient interaction of ISCU with the β3-β5 sheet of FXN, previously proposed for the interaction between the two proteins, could affect the structure and/or dynamics of the iron-binding region. Moreover, differently from what observed before by Cai and coworkers [34], the finding that upon addition of ISCU the spectrum of FXN remained very similar to that of the iron-bound protein indicates that, at least in our conditions, the transfer of iron from FXN to ISCU does not take place. Qualitatively similar results were obtained when N-6his-tagged ISCU was added to the FXN mutants studied in this work in the presence of 4 equivalents of Fe^{2+}, in anaerobic conditions. As in the case of the wild type FXN, the addition of N-6his-tagged ISCU causes changes in the NMR spectra for peaks corresponding to residues in the α1/β1 acidic region, mostly in term of a further line broadening (Fig. 7). This was not evident in the case of G130V, where the signals that experienced the larger effect in presence of ISCU for the wild type FXN or for the mutants were already extremely broad upon iron addition. Although there are some small differences, in all cases the addition of ISCU appeared to strengthen the effects observed upon addition of iron. In particular, there are 8 peaks, corresponding to E108, E111, D112, L113, D115, V125 and S126, that disappear or become very weak upon addition of Fe^{2+} and ISCU. Interestingly, they are located in

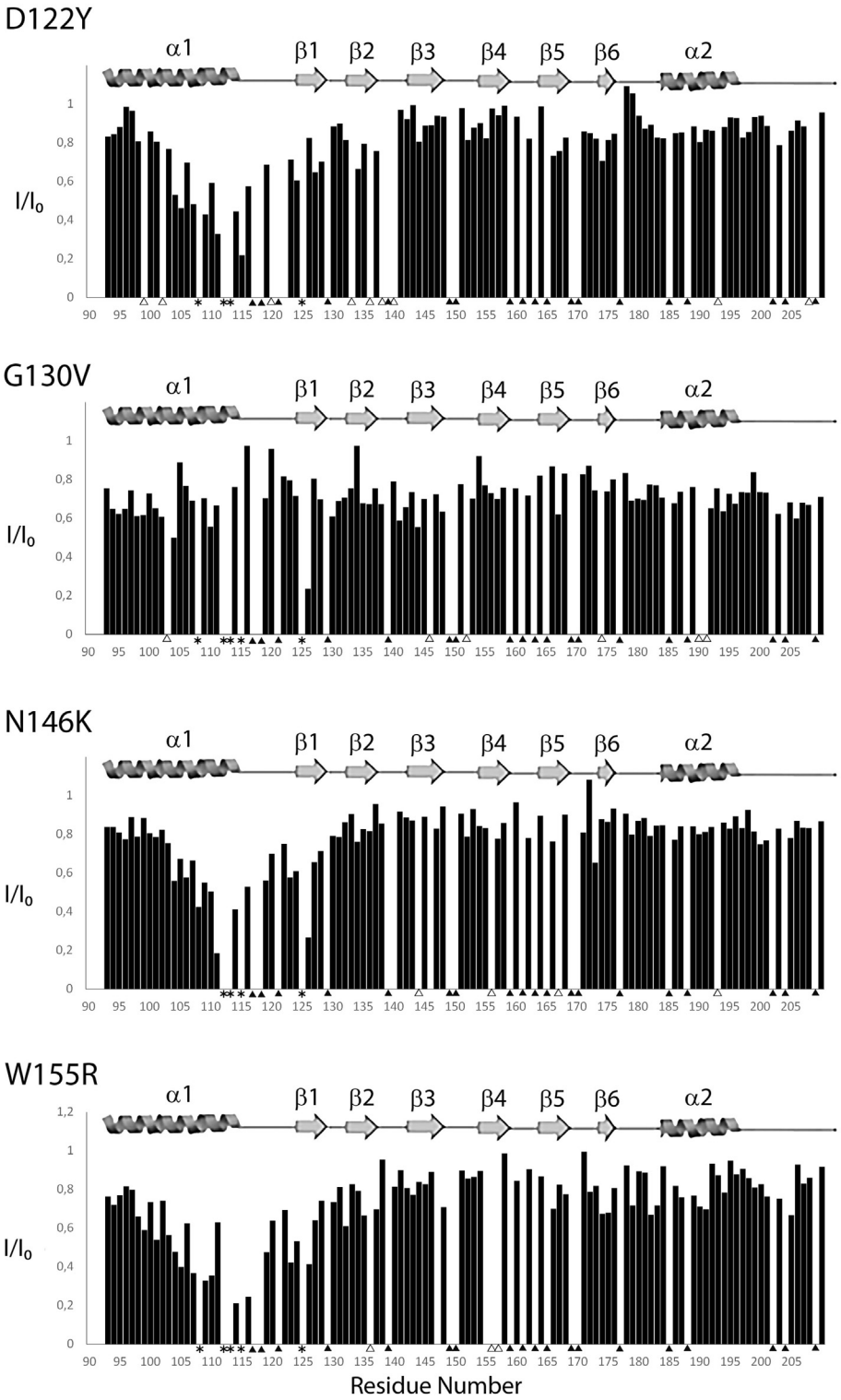

Fig. 7. Ratios of the peak intensities in the spectra without (I_0) and with (I) ISCU represented as a function of the residue number for FXN mutants. Residues corresponding to signals which disappeared in presence of ISCU and iron are indicated with asterisks. Prolines or residues corresponding to severe overlapped or unassigned peaks in wild type FXN are marked with black triangles while residues which cannot be traced in the mutants are shown with empty triangles. A schematic representation of FXN secondary structure is inserted in frame with residues sequence number to facilitate the interpretation of the figure.

the C-terminal part of α1 and in the resides of β1 facing it, while the binding sites at the N-terminus of α1 and in the loop are much less influenced.

In order to exclude that the effect of ISCU on FXN described above may be due to an interaction of the N-terminal 6his-tag, possibly mediated by iron, we produced a novel construct allowing the expression of a C-6his-ISCU protein, with a TEV-cleavage site to remove the tag after purification, as described in Materials and methods and in the supplementary materials. The C-6his-ISCU and untagged ISCU proteins were then used to explore potential effects on the NMR spectrum of the iron-bound ^{15}N-labeled frataxin, exactly as described above. We found that both proteins did not cause neither evident chemical

shift perturbation nor additional broadening of NMR signals, including those corresponding to the residues of the α1/β1 acidic already perturbed by iron-binding, unlike what we observed with the N-6his-tagged ISCU protein (supplementary Fig. S10). On the other hand, the lack of effects observed with untagged or C-6his-tagged ISCU proteins suggested that the his-tag at the N-terminus should influence the structural properties of ISCU. In view of the capability of ISCU to explore different conformational states, as previously reported by different groups [65,66], it is likely that the flexible N-terminus when his-tagged promotes a shift of the equilibrium among conformations. Thus, a transient interaction between FXN and ISCU could be enhanced, allowing the changes measured in the NMR spectra. In particular, the significant increase of line broadening for residues in the α1/β1 acidic region already perturbed by iron-binding could be due to an enhancement of paramagnetic Curie relaxation caused by existence of transient, low population of the complex between the two proteins.

Taken together, these results confirm that a binary complex interaction between FXN and ISCU, at least in the absence of the other ISC complex functional partners, is not formed, as it was pointed out by Cai and co-workers with the $FXN_{80–210}$ protein [34]. On the other hand, they suggest that the presence of a 6his-tag at the N-terminus of ISCU may promote a transient interaction with FXN, which is not mediated by a potential iron-binding to the 6his-tag.

The capability of iron-bound FXN to functionally interact with the NFS1-ISD11-ACP-ISCU complex is pivotal to drive the biogenesis of the FeS clusters at the assembly machinery. The mutations of the highly conserved residues associated with the four clinical variants analyzed in this work are all expected to have a functional impact on the FeS clusters synthesis. Since our EPR and NMR data did not point out significant differences between the wild type and the mutant proteins in terms of iron-binding and ISCU interaction, to further investigate the structure-function relationships in these variants we next evaluated their activity at the whole FeS cluster biogenesis complex. Mammalian FXN was proposed to stimulate the rate of FeS clusters assembly by enhancing the sulfide production at the NFS1-ISD11-ISCU machinery [53,67,68]. The cysteine desulfurase NFS1, which forms a functional complex with ISD11 (an essential mitochondrial matrix protein that is required for the stability and function of NFS1), catalyzes the breakdown of cysteine to alanine and produces a transient persulfide species that can be detected *in vitro* by the enzymatic assay described in detail in Materials and methods. By taking advantage of this approach, we monitored the amount of sulfide produced by NFS1/ISD11 conversion of cysteine to alanine in the presence of ISCU, with or without wild type or mutant frataxin proteins. In these experiments, sulfide production has been monitored in the presence of 1 equivalent of the NFS1/ISD11 complex, purified as described in Materials and methods, 3 equivalents of ISCU and 10 equivalents of Fe^{2+}, either in the absence or in the presence of wild type FXN and of each of the four FXN variants. The results of these analyses are reported in Fig. 8 and Table 3 in Supplementary material. The mutations N146K and W155R had been previously shown to affect the capability of FXN to stimulate the NFS1/ISD11 desulfurase activity *in vitro* [48,69], whereas these data were lacking for both D122Y and G130V variants. Our results confirmed that i) wild type FXN increases the cysteine desulfurase activity of NFS1/ISD11 complex and ii) N146K and W155R variants are almost unable to further activate NFS1. We next analyzed the effects of G130 V and D122Y point mutations. We found that, when compared to the wild type FXN, both variants retain a partial capability to enhance the desulfurase activity *in vitro*. Since it has been previously proposed the FXN stimulatory effect on the desulfurase activity relies on the presence of the ISCU scaffold [68], these functional data would be in accordance with the structural NMR analysis reported above. On the other hand, even though N146K may be more stable than the wild type protein, it exhibited a significant decrease of desulfurase activation. Based on the analysis of the experimental model of NFS1/ISD11-ACP/ISCU/FXN complex determined by Cai and coworkers [34], residue Asn146 of FXN interacts with residues Pro108 and Val109 of ISCU (supplementary Fig. S11). Thus, the mutation N146K may distort the interaction surface of ISCU-FXN subcomplex. In fact, when the residue is mutated to Lys, the N atom of the Lys146 side-chain is located near Cys44 of ISCU (*i.e.* 5.0–6.0 Å), one of the conserved Cys residues where the cluster is assembled. Therefore, the electrostatics of the active site of ISCU (residues Cys44, Cys70, His112 and Cys113) may be highly altered by the presence of a positive charge.

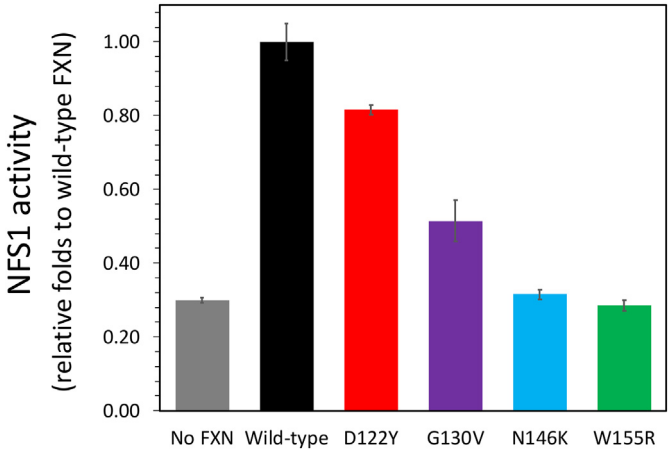

Fig. 8. Modulation of the NFS1 cysteine desulfurase activity at the FeS clusters assembly complex. Sulfide production was assessed in the presence of 1 equivalent of the NFS1/ISD11 complex, 3 equivalents of ISCU and 10 Fe^{2+} equivalents, either in the absence or in the presence of 3 equivalents of wild type FXN and each FXN mutant, as described in detail in Materials and methods. The enzymatic activity is normalized to the desulfurase activity in the presence of wild type FXN. Data represent the mean of three replicates ± S.D.

Taken together, these data thus indicate that iron-binding, at least to the specific FXN clinical variants selected in this work, is not univocally related to their capability to enhance sulfide production *via* binding the NFS1-ISD11-ISCU complex, one the proposed molecular functions of frataxin. The complex relationships between stability and function of FXN at the whole FeS cluster assembly machinery are currently under further investigation in our laboratory.

4. Conclusions

One of the end results of FXN decrease in cells of FRDA patients is a severe iron overload in their mitochondria, especially in nerve and cardiac tissues, associated to cellular iron dysregulation, impairment of FeS clusters assembly and increased sensitivity to oxidative stress, likely due to the mitochondrial redox-active environment. This has been suggested to play a key role in the pathogenesis of the disease and indeed pharmacological strategies based on free-radical scavengers, such as idebenone or CoQ_{10}, as well as on iron chelators, such as deferiprone, showed some cardiac and neurological improvements in FRDA mouse models and in-patient clinical trials [11,70–72]. On the other hand, to date the primary cause of the disease is still difficult to identify, and the precise physiological role of FXN remains unclear, both in iron metabolism and in the FeS clusters biogenesis. Although iron-binding to FXN has been proposed to be essential for its function(s), this important issue is still controversial in many respects, and has been readdressed in the present work in which we combined different advanced spectroscopic analyses to investigate the iron-binding properties of a recombinant human FXN. Moreover, in order to disclose potential structure-function relationships, we applied the same multidisciplinary approach to a panel of FXN variants found in FRDA heterozygous patients, with point mutations in highly conserved residues mapping either in the iron-binding acidic ridge or in the surface involved in the iron-dependent interaction of FXN with the FeS clusters assembly

machinery. EPR is an advanced spectroscopic technique of choice to investigate metalloproteins, and in this work it has been exploited for the first time to provide direct experimental evidence *in vitro* that FXN binds Fe^{3+}. This was then further supported by 2D NMR experiments, which also confirmed that FXN is able to bind iron ions in both oxidation states, although with slightly different binding modes. An intriguing result was obtained by the same NMR analysis when iron-bound FXN was incubated with ISCU, the scaffold protein of the mitochondrial FeS clusters assembly machinery, providing a novel molecular insight on this complex biosynthetic pathway: indeed, our data may suggest that structural changes of the N-terminal portion of ISCU could be instrumental for the transitions between different conformational states, which have been previously claimed to be relevant, as scaffold protein, for the interactions with the functional partners of the FeS cluster assembly machinery [65,66].

Although the pathophysiological consequences of the point mutations of the selected variants are relevant, no significant differences were detected when compared to the wild type FXN, in terms of both iron-binding properties and interaction with the ISCU scaffold protein, suggesting that these are not key factors for the disease onset, at least in heterozygous patients. On the other hand, we confirmed that two out the four FXN mutants (*i.e.* N146K and W155R) have an impaired capability to enhance the desulfurase activity *in vitro*, one of the functional roles that have been hypothesized for this protein. This indicates that FXN missense point mutations could have multiple biochemical effects, and further supports the multifunctional nature of the protein. Examining FXN mutations in the context of protein structure/function relationships is expected to increase our knowledge of FXN biology and FRDA pathology, and additional clinical mutants are thus currently under investigation in our laboratory.

Understanding the intricate pathophysiology of FXN defects is pivotal to characterize the FRDA disease molecular mechanisms and to better define the clinical outcome of both homozygous and compound heterozygous patients, which is in turn crucial to develop novel, more specific therapeutic strategies.

Supplementary data to this article can be found online at https://doi.org/10.1016/j.bbapap.2019.07.007.

Declaration of Competing Interest

None

Acknowledgements

This work was supported by grants COST_FINA_P14_02 to Paola Costantini from Department of Biology, University of Padova; Fondazione Cassa di Risparmio di Padova e Rovigo (CARIPARO) starting grants to Donatella Carbonera and Marco Bortolus; PICT 2016 2280 from ANPCyT (Argentina) and Friedreich's Ataxia Research Alliance (FARA) to Javier Santos. Massimo Bellanda acknowledges the financial support by grant P-DiSC #01BIRD2018-UNIPD from University of Padova. We especially thank Dr. Hélène Puccio and Dr. Benoit D'Autréaux for kindly providing us with the *FXN* and *NFS1/ISD11* genes, respectively.

References

[1] S. Adinolfi, M. Trifuoggi, A.S. Politou, S. Martin, A. Pastore, A structural approach to understanding the iron-binding properties of phylogenetically different frataxins, Hum. Mol. Genet. 11 (2002) 1865–1877.
[2] T.J. Gibson, E.V. Koonin, G. Musco, A. Pastore, P. Bork, Friedreich's ataxia protein: phylogenetic evidence for mitochondrial dysfunction, Trends Neurosci. 19 (1996) 465–468.
[3] V. Campuzano, L. Montermini, M.D. Molto, L. Pianese, M. Cossée, F. Cavalcanti, E. Monros, F. Rodius, F. Duclos, A. Monticelli, F. Zara, J. Canizares, H. Koutnikova, S.I. Bidichandani, C. Gellera, A. Brice, P. Trouillas, G. De Michele, A. Filla, R. De Frutos, F. Palau, P.I. Patel, S. Di Donato, J.L. Mandel, S. Cocozza, M. Koenig, M. Pandolfo, Friedreich's ataxia: autosomal recessive disease caused by an intronic GAA triplet repeat expansion, Science 271 (1996) 1423–1427.
[4] V. Campuzano, L. Montermini, Y. Lutz, L. Cova, C. Hindelang, S. Jiralerspong, Y. Trottier, S.J. Kish, B. Faucheux, P. Trouillas, F.J. Authier, A. Dürr, J.L. Mandel, A. Vescovi, M. Pandolfo, M. Koenig, Frataxin is reduced in Friedreich ataxia patients and is associated with mitochondrial membrane, Hum. Mol. Genet. 6 (1997) 1771–1780.
[5] M. Pandolfo, Friedreich ataxia: the clinical picture, J. Neurol. 256 (2009) 3–8.
[6] M. Cossée, A. Dürr, M. Schmitt, N. Dahl, P. Trouillas, P. Allinson, M. Kostrzewa, A. Nivelon-Chevallier, K.H. Gustavson, A. Kohlschütter, U. Müller, J.L. Mandel, A. Brice, M. Koenig, F. Cavalcanti, A. Tammaro, G. De Michele, A. Filla, S. Cocozza, M. Labuda, L. Montermini, J. Poirier, M. Pandolfo, Friedreich's ataxia: point mutations and clinical presentation of compound heterozygotes, Ann. Neurol. 45 (1999) 200–206.
[7] M. De Castro, J. García-Planells, E. Monrós, J. Cañizares, R. Vázquez-Manrique, J.J. Vílchez, M. Urtasun, M. Lucas, G. Navarro, G. Izquierdo, M.D. Moltó, F. Palau, Genotype and phenotype analysis of Friedreich's ataxia compound heterozygous patients, Hum. Genet. 106 (2000) 86–92.
[8] C. Gellera, B. Castellotti, C. Mariotti, R. Mineri, V. Seveso, S. Di Donato, F. Taroni, Frataxin gene point mutations in Italian Friedreich ataxia patients, Neurogenetics 8 (2007) 289–299.
[9] A.R. Correia, S. Adinolfi, A. Pastore, C.M. Gomes, Conformational stability of human frataxin and effect of Friedreich's ataxia related mutations on protein folding, Biochem. J. 398 (2006) 605–611.
[10] A.R. Correia, C. Pastore, S. Adinolfi, A. Pastore, C.M. Gomes, Dynamics, stability and iron-binding activity of frataxin clinical mutants, FEBS J. 275 (2008) 3680–3690.
[11] S. Schmucker, H. Puccio, Understanding the molecular mechanisms of Friedreich's ataxia to develop therapeutic approaches, Hum. Mol. Genet. 19 (2010) R103–R110.
[12] M. Pandolfo, A. Pastore, The pathogenesis of Friedreich ataxia and the structrure and function of frataxin, J. Neurol. 256 (Suppl. 1) (2009) 9–17.
[13] T. Yoon, J.A. Cowan, Frataxin-mediated iron delivery to ferrochetalase in the final step of heme biosynthesis, J. Biol. Chem. 279 (2004) 25943–25946.
[14] M.A. Huynen, B. Snel, P. Bork, T.J. Gibson, The phylogenetic distribution of frataxin indicates a role in iron-sulfur cluster protein assembly, Hum. Mol. Genet. 10 (2001) 2463–2468.
[15] P. Cavadini, H.A. O'Neill, O. Benada, G. Isaya, Assembly and iron-binding properties of human frataxin, the protein deficient in Friedreich ataxia, Hum. Mol. Genet. 11 (2002) 217–227.
[16] T. Yoon, J.A. Cowan, Iron-sulfur cluster biosynthesis. Characterization of frataxin as an iron donor for assembly of [2Fe-2S] clusters in ISU-type proteins, J. Am. Chem. Soc. 125 (2003) 6078–6084.
[17] A. Rötig, P. de Lonlay, D. Chretien, F. Foury, M. Koenig, D. Sidi, A. Munnich, P. Rustin, Aconitase and mitochondrial iron-Sulphur protein deficiency in Friedreich ataxia, Nat. Genet. 17 (1997) 215–217.
[18] H. Puccio, D. Simon, M. Cossée, P. Criqui-Filipe, F. Tiziano, J. Melki, C. Hindelang, R. Matyas, P. Rustin, M. Koenig, Mouse models for Friedreich ataxia exhibit cardiomyopathy, sensory nerve defect and Fe-S enzyme deficiency followed by intramitochondrial iron deposits, Nat. Genet. 27 (2001) 181–186.
[19] J.B. Schulz, T. Dehmer, L. Schols, H. Mende, C. Hardt, M. Vorgerd, K. Burk, W. Matson, J. Dichgans, M.F. Beal, M.B. Bogdanov, Oxidative stress in patients with Friedreich's ataxia, Neurology 55 (2000) 1719–1721.
[20] R.V. Vaubel, G. Isaya, Iron-sulfur cluster synthesis, iron homeostasis and oxidative stress in Friedreich ataxia, Mol. Cell. Neurosci. 55 (2013) 50–61.
[21] A. Martelli, M. Wattenhofer-Donze, S. Schmucker, S. Bouvet, L. Reutenauer, H. Puccio, Frataxin is essential for extramitochondrial Fe-S cluster proteins in mammalian tissues, Hum. Mol. Genet. 16 (2007) 2651–2658.
[22] M.L. Huang, E.M. Becker, M. Whitnall, Y.S. Rahmanto, P. Ponka, D.R. Richardson, Elucidation of the mechanism of mitochondrial iron loading in Friedreich's ataxia by analysis of a mouse mutant, Proc. Natl. Acad. Sci. U. S. A. 106 (2009) 16381–16386.
[23] M. Whitnall, Y.S. Rahmanto, R. Sutak, X. Xu, E.M. Becker, M.R. Mikhael, P. Ponka, D.R. Richardson, The MCK mouse heart model of Friedreich's ataxia: alterations in iron-regulated proteins and cardiac hypertrophy are limited by iron chelation, Proc. Natl. Acad. Sci. U. S. A. 105 (2008) 9757–9762.
[24] H. Koutnikova, V. Campuzano, M. Koenig, Maturation of wild-type and mutated frataxin by the mitochondrial processing peptidase, Hum. Mol. Genet. 7 (1998) 1485–1489.
[25] I. Condò, N. Ventura, F. Malisan, A. Rufini, B. Tomassini, R. Testi, *In vivo* maturation of human frataxin, Hum. Mol. Genet. 16 (2007) 1534–1540.
[26] S. Schmucker, M. Argentini, N. Carelle-Camels, A. Martelli, H. Puccio, The *in vivo* mitochondrial two-steps maturation of human frataxin, Hum. Mol. Genet. 17 (2008) 3521–3531.
[27] G. Musco, G. Stier, B. Kolmerer, S. Adinolfi, S.R. Martin, T.A. Frenkiel, T.J. Gibson, A. Pastore, Towards a structural understanding of Friedreich's ataxia: the solution structure of frataxin, Structure 8 (2000) 695–707.
[28] S. Dhe-Paganon, R. Shigeta, Y.I. Chi, M. Ristow, S.E. Shoelson, Crystal structure of human frataxin, J. Biol. Chem. 275 (2000) 30753–30756.
[29] M. Nair, S. Adinolfi, C. Pastore, G. Kelly, P. Temussi, A. Pastore, Solution structure of the bacterial frataxin ortholog, CyaY: mapping the iron binding sites, Structure 12 (2004) 2037–2048.
[30] Y. He, S.L. Alam, S.V. Proteasa, Y. Zhang, E. Lesuisse, A. Dancis, T.L. Stemmler, Yeast frataxin solution structure, iron binding, and ferrochetalase interaction, Biochemistry 43 (2004) 16254–16262.
[31] J.D. Cook, K.Z. Bencze, A.D. Jankovic, A.K. Crater, C.N. Busch, P.B. Bradley, A.J. Stemmler, M.R. Spaller, T.L. Stemmler, Monomeric yeast frataxin is an iron-binding protein, Biochemistry 45 (2006) 7767–7777.

[32] L.E. Gentry, M.A. Thacker, R. Doughty, R. Timkovich, L.S. Busenlehner, His86 from the N-terminus of frataxin coordinates iron and is required for Fe-S cluster synthesis, Biochemistry 52 (2013) 6085–6096.
[33] J. Huang, E. Dizin, J. Cowan, Mapping iron binding sites on human frataxin: implications for cluster assembly on the ISCU Fe-S cluster scaffold protein, J. Biol. Inorg. Chem. 13 (2008) 825–836.
[34] K. Cai, R.O. Frederick, M. Tonelli, J.L. Markley, Interactions of iron-bound frataxin with ISCU and ferredoxin on the cysteine desulfurase complex leading to Fe-S cluster assembly, J. Inorg. Biochem. 183 (2018) 107–116.
[35] E.A. Roman, S.E. Faraj, M. Gallo, A.G. Salvay, D.U. Ferreiro, J. Santos, Protein stability and dynamics modulation: the case of human frataxin, PLoS One 7 (2012) e45743.
[36] Z. Marelja, W. Stocklein, M. Nimtz, S. Leimkühler, A novel role for human Nfs1 in the cytoplasm: Nfs1 acts as a sulfur donor for MOCS3, a protein involved in molybdenum cofactor biosynthesis, J. Biol. Chem. 283 (2008) 25178–25185.
[37] G. Bohm, R. Muhr, R. Jaenicke, CDNN: quantitative analysis of protein far UV circular dichroism spectra by neural networks, Protein Eng. 5 (1992) 191–195.
[38] P. Schanda, B. Brutscher, Very fast two-dimensional NMR spectroscopy for real-time investigation of dynamic events in proteins on the time scale of seconds, J. Am. Chem. Soc. 127 (2005) 8014–8015.
[39] W. Lee, M. Tonelli, J.L. Markley, NMRFAM-SPARKY: enhanced software for biomolecular NMR spectroscopy, Bioinformatics 31 (2015) 1325–1327.
[40] R. Keller, The Computer Aided Resonance Assignment Tutorial, 1st, (2004) ISBN 3-85600-112-113.
[41] W.L. DeLano, Pymol: an open-source molecular graphics tool, CCP4 Newsletter on Protein Crystallography 40 (2002) 82–92.
[42] T. Yoon, E. Dizin, J.A. Cowan, N-terminal iron-mediated self-cleavage of human frataxin: regulation of iron binding and complex formation with target proteins, J. Biol. Inorg. Chem. 12 (2007) 535–542.
[43] D.J. Lane, D.R. Richardson, Frataxin, a molecule of mystery: trading stability for function in its iron-binding site, Biochem. J. 426 (2010) e1–e3.
[44] G. Musco, T. DeTommasi, G. Stier, B. Kolmerer, M. Bottomley, S. Adinolfi, F. Muskett, T. Gibson, T. Frenkiel, A. Pastore, Assignment of the ^{1}H, ^{15}N, and ^{13}C resonances of the C-terminal domain of frataxin, the protein responsible for Friedreich ataxia, J. Biomol. NMR 15 (1999) 87–88.
[45] F. Bou-Abdallah, S. Adinolfi, A. Pastore, T.M. Laue, N. Dennis Chasteen, Iron binding and oxidation kinetics in frataxin CyaY of *Escherichia coli*, J. Mol. Biol. 341 (2004) 605–615.
[46] A. Ilari, M.C. Latella, P. Ceci, F. Ribacchi, M. Su, L. Giangiacomo, S. Stefanini, N.D. Chasteen, E. Chiancone, The unusual intersubunit ferroxidase center of *Listeria innocua* Dps is required for hydrogen peroxide detoxification but not for iron uptake. A study with site-specific mutants, Biochemistry 44 (2005) 5579–5587.
[47] F. Bou-Abdallah, N.D. Chasteen, Spin concentration measurements of high-spin (g' = 4.3) rhombic iron(III) ions in biological samples: theory and application, J. Biol. Inorg. Chem. 13 (2008) 15–24.
[48] C.L. Tsai, J. Bridwell-Rabb, D.P. Barondeau, Friedreich's ataxia variants I154F and W155R diminish frataxin-based activation for the iron-sulfur cluster assembly complex, Biochemistry 50 (2011) 6478–6487.
[49] J. Gerber, U. Mühlenhoff, R. Lill, An interaction between frataxin and Isu1/Nfs1 that is crucial for Fe/S cluster synthesis on Isu1, EMBO Rep. 4 (2003) 906–911.
[50] H. Li, O. Gakh, D.Y. Smith IV, G. Isaya, Oligomeric yeast frataxin drives assembly of core machinery for mitochondrial iron-sulfur cluster synthesis, J. Biol. Chem. 284 (2009) 21971–21980.
[51] C.L. Tsai, D.P. Barondeau, Human frataxin is an allosteric switch that activates the Fe-S cluster biosynthetic complex, Biochemistry 49 (2010) 9132–9139.
[52] J. Bridwell-Rabb, C. Iannuzzi, A. Pastore, D.P. Barondeau, Effector role reversal during evolution: the case of frataxin in Fe-S cluster biosynthesis, Biochemistry 51 (2012) 2506–2514.
[53] A. Parent, X. Elduque, D. Cornu, L. Belot, J.-P. Le Caer, A. Grandas, M.B. Toledano, B. D'Autréaux, Mammalian frataxin directly enhances sulfur transfer of NFS1 persulfide to both ISCU and free thiols, Nat. Commun. 6 (2015) 5686.
[54] R. Lill, Function and biogenesis of iron-sulphur proteins, Nature 460 (2009) 831–838.
[55] R. Lill, U. Mühlenhoff, Maturation of iron-sulfur proteins in eukaryotes: mechanisms, connected processes, and diseases, Annu. Rev. Biochem. 77 (2008) 669–700.
[56] J.G. Van Vranken, M.Y. Jeong, P. Wei, Y.C. Chen, S.P. Gygi, D.R. Winge, J. Rutter, The mitochondrial acyl carrier protein (ACP) coordinates mitochondrial fatty acid synthesis with iron sulfur cluster biogenesis, Elife 5 (2016) e17828.
[57] S.A. Cory, J.G. Van Vranken, E.J. Brignole, S. Patra, D.R. Winge, C.L. Drennan, J. Rutter, D.P. Barondeau, Structure of human Fe-S assembly subcomplex reveals unexpected cysteine desulfurase architecture and acyl-ACP-ISD11 interactions, Proc. Natl. Acad. Sci. U. S. A. 114 (2017) E5325–E5334.
[58] M.T. Boniecki, S.A. Freibert, U. Mühlenhoff, R. Lill, M. Cygler, Structure and functional dynamics of the mitochondrial Fe/S cluster synthesis complex, Nat. Commun. 8 (2017) 1287.
[59] K. Cai, R.O. Frederick, H. Dashti, J.L. Markley, Architectural features of human mitochondrial cysteine desulfurase complexes from crosslinking mass spectrometry and small-angle X-ray scattering, Structure 26 (2018) 1127–1136.
[60] N.G. Fox, X. Yu, X. Feng, H.J. Bailey, A. Mertelli, J.F. Nabhan, C. Strain-Damerell, C. Bulawa, W.W. Yue, S. Han, Structure of the human frataxin-bound iron-sulfur cluster assembly complex provides insight into its activation mechanism, Nat. Commun. 10 (2019) 2210.
[61] A. Martelli, M. Wattenhofer-Donzé, S. Schmucker, S. Bouvet, L. Reutenauer, H. Puccio, Frataxin is essential for extramitochondrial Fe-S cluster proteins in mammalian tissues, Hum. Mol. Genet. 16 (2007) 2651–2658.
[62] S. Schmucker, A. Martelli, F. Colin, A. Page, M. Wattenhofer-Donzé, L. Reutenauer, H. Puccio, Mammalian frataxin: an essential function for cellular viability through an interaction with a preformed ISCU/NFS1/ISD11 iron-sulfur assembly complex, PLoS One 6 (2011) e16199.
[63] Y. Shan, E. Napoli, G. Cortopassi, Mitochondrial frataxin with ISD11 of the NFS1/ISCU complex and multiple mitochondrial chaperones, Hum. Mol. Genet. 16 (2007) 929–941.
[64] S. Leidgens, S. De Smet, F. Foury, Frataxin interacts with Isu1 through a conserved tryptophan in its beta-sheet, Hum. Mol. Genet. 19 (2010) 276–286.
[65] J.H. Kim, J.L. Tonelli, J.L. Markley, Disordered form of the scaffold protein IscU in the substrate for iron-sulfur cluster on cysteine desulfurase, Proc. Natl. Acad. Sci. U. S. A. 109 (2012) 454–459.
[66] R. Yan, G. Kelly, A. Pastore, The scaffold protein IscU retains a structured conformation in the FeS cluster assembly complex, ChemBioChem 15 (2014) 1682–1686.
[67] F. Colin, A. Martelli, M. Clémancey, J.M. Latour, S. Gambarelli, L. Zeppieri, C. Birck, A. Page, H. Puccio, S. Ollagnier de Choudens, Mammalian frataxin controls sulfur production and iron entry during *de novo* Fe4S4 cluster assembly, J. Am. Chem. Soc. 135 (2013) 733–740.
[68] J. Bridwell-Rabb, N.G. Fox, C.L. Tsai, A.M. Winn, D.P. Barondeau, Human frataxin activates Fe-S cluster biosynthesis by facilitating sulfur transfer chemistry, Biochemistry 53 (2014) 4904–4913.
[69] J. Bridwell-Rabb, A.M. Winn, D.P. Barondeau, Structure-function analysis of Friedreich's ataxia mutants reveals determinants of frataxin binding and activation of the Fe-S assembly complex, Biochemistry 50 (2011) 7265–7274.
[70] H. Seznec, D. Simon, L. Monassier, P. Criqui-Filipe, A. Gansmuller, P. Rustin, M. Koenig, H. Puccio, Idebenone delays the onset of cardiac functional alteration without correction of Fe-S enzymes deficit in a mouse model for Friedreich ataxia, Hum. Mol. Genet. 13 (2004) 1017–1024.
[71] P.E. Hart, R. Lodi, B. Rajagopalan, J.L. Bradley, J.G. Crilley, C. Turner, A.M. Blamire, D. Manners, P. Styles, A.H. Schapira, J.M. Cooper, Antioxidant treatment of patients with Friedreich ataxia: four-year follow-up, Arch. Neurol. 62 (2005) 621–626.
[72] N. Boddaert, K.H. Le Quan Sang, A. Rötig, A. Leroy-Willig, S. Gallet, F. Brunelle, D. Sidi, J.C. Thalabard, A. Munnich, Z.I. Cabantchik, Selective iron chelation in Friedreich ataxia: biologic and clinical implications, Blood 110 (2007) 401–408.